AMERICAN SOCIETY FOR MICROBIOLOGY | Antimicrobial Agents and Chemotherapy®

MECHANISMS OF RESISTANCE

Structural and Biochemical Characterization of the Novel CTX-M-151 Extended-Spectrum β-Lactamase and Its Inhibition by Avibactam

Barbara Ghiglione,[a,b,c] María Margarita Rodríguez,[a,b,c] Florencia Brunetti,[a,b,c] Krisztina M. Papp-Wallace,[d,e,f,g] Ayumi Yoshizumi,[h] Yoshikazu Ishii,[h] Robert A. Bonomo,[d,e,f,g] Gabriel Gutkind,[a,b,c] Sebastián Klinke,[i] Pablo Power[a,b,c]

[a]Universidad de Buenos Aires, Facultad de Farmacia y Bioquímica, Departamento de Microbiología, Inmunología y Biotecnología, Laboratorio de Resistencia Bacteriana, Buenos Aires, Argentina
[b]Consejo Nacional de Investigaciones Científicas y Técnicas (CONICET), Buenos Aires, Argentina
[c]Instituto de Investigaciones en Bacteriología y Virología Molecular (IBaViM), Buenos Aires, Argentina
[d]Research Service, Louis Stokes Cleveland Department of Veterans Affairs, Cleveland, Ohio, USA
[e]Department of Medicine, Case Western Reserve University, Cleveland, Ohio, USA
[f]Center for Proteomics and Bioinformatics, Case Western Reserve University, Cleveland, Ohio, USA
[g]Department of Biochemistry, Case Western Reserve University, Cleveland, Ohio, USA
[h]Department of Microbiology and Infectious Diseases, Toho University, Tokyo, Japan
[i]Fundación Instituto Leloir, IIBBA-CONICET, and Plataforma Argentina de Biología Estructural y Metabolómica PLABEM, Buenos Aires, Argentina

Sebastián Klinke and Pablo Power contributed equally to this work.

ABSTRACT The diazabicyclooctane (DBO) inhibitor avibactam (AVI) reversibly inactivates most serine β-lactamases, including the CTX-M β-lactamases. Currently, more than 230 unique CTX-M members distributed in five clusters with less than 5% amino acid sequence divergence within each group have been described. Recently, a variant named CTX-M-151 was isolated from a *Salmonella enterica* subsp. *enterica* serovar Choleraesuis strain in Japan. This variant possesses a low degree of amino acid identity with the other CTX-Ms (63.2% to 69.7% with respect to the mature proteins), and thus it may represent a new subgroup within the family. CTX-M-151 hydrolyzes ceftriaxone better than ceftazidime (k_{cat}/K_m values 6,000-fold higher), as observed with CTX-Ms. CTX-M-151 is well inhibited by mechanism-based inhibitors like clavulanic acid (inactivation rate [k_{inact}]/inhibition constant [K_i] = 0.15 $\mu M^{-1} \cdot s^{-1}$). For AVI, the apparent inhibition constant ($K_{i\ app}$), 0.4 μM, was comparable to that of KPC-2; the acylation rate (k_2/K) (37,000 $M^{-1} \cdot s^{-1}$) was lower than that for CTX-M-15, while the deacylation rate (k_{off}) (0.0015 s^{-1}) was 2- to 14-fold higher than those of other class A β-lactamases. The structure of the CTX-M-151/AVI complex (1.32 Å) reveals that AVI adopts a chair conformation with hydrogen bonds between the AVI carbamate and Ser70 and Ser237 at the oxyanion hole. Upon acylation, the side chain of Lys73 points toward Ser130, which is associated with the protonation of Glu166, supporting the role of Lys73 in the proton relay pathway and Glu166 as the general base in deacylation. To our knowledge, this is the first chromosomally encoded CTX-M in *Salmonella* Choleraesuis that shows similar hydrolytic preference toward cefotaxime (CTX) and ceftriaxone (CRO) to that toward ceftazidime (CAZ).

KEYWORDS DBO, ESBL, *Salmonella* Choleraesuis, X-ray crystallography, cefotaximase, phylogeny

Antimicrobial resistance (AMR) has emerged as one of the leading public health crises of the 21st century, and with the rise of multidrug-resistant (MDR) bacteria, health care providers are presented with major clinical challenges. Among these, finding

Citation Ghiglione B, Rodríguez MM, Brunetti F, Papp-Wallace KM, Yoshizumi A, Ishii Y, Bonomo RA, Gutkind G, Klinke S, Power P. 2021. Structural and biochemical characterization of the novel CTX-M-151 extended-spectrum β-lactamase and its inhibition by avibactam. Antimicrob Agents Chemother 65:e01757-20. https://doi.org/10.1128/AAC.01757-20.

Address correspondence to Sebastián Klinke, sklinke@leloir.org.ar, or Pablo Power, ppower@ffyb.uba.ar.

Received 13 August 2020
Returned for modification 19 October 2020
Accepted 28 December 2020
Accepted manuscript posted online 11 January 2021
Published 18 March 2021

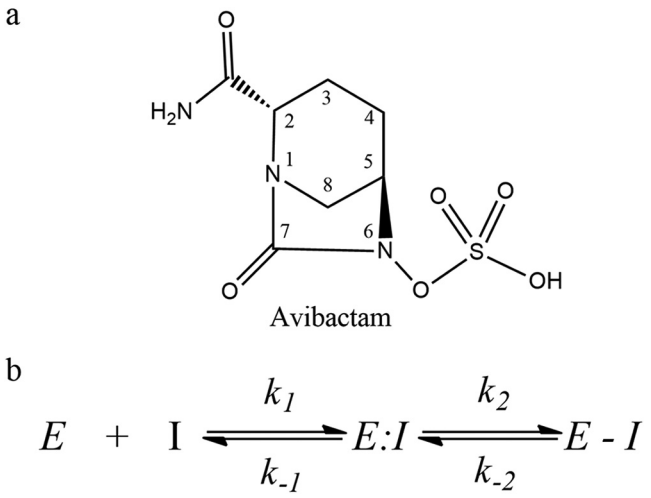

FIG 1 (a) Chemical structure of avibactam (AVI). (b) Kinetic model of the interaction of a serine β-lactamase with AVI.

pharmacologic alternatives to expand the available arsenal to combat bacterial infections caused by pathogens producing increasingly specialized β-lactamases is mandatory.

Avibactam (AVI) is a bridged bicyclic ((2*S*,5*R*)-7-oxo-6-(sulfooxy)-1,6-diazabicyclo[3,2,1] octane-2carboxamide) (DBO) non-β-lactam β-lactamase inhibitor (BLI) (Fig. 1a) that reversibly inactivates most Ambler class A and C β-lactamases and some class D enzymes (1). AVI follows two routes toward diacylation; the major route is recyclization via ring closure (i.e., regenerating the intact AVI). Thus, AVI may acylate other β-lactamase molecules (Fig. 1b) (2–6). This reversibility is the main difference between the inactivation of β-lactamases by AVI and the inactivation mechanisms by other BLIs such as tazobactam, sulbactam, and clavulanic acid. These latter BLIs inactivate via a nucleophilic attack by the active site serine on the amide bond of the BLI, acylation of the enzyme, and subsequent rearrangement steps resulting in imine or enamine intermediates, inhibitor fragmentation, and a transient or long-term inhibition of the enzyme (7). Despite these differences, AVI shares some mechanistic similarities with other inhibitors, namely, a carbonyl carbon atom, acylation of Ser70, and accommodation of the carbonyl oxygen in the oxyanion hole for stabilization of the transition state (3).

Several crystallographic structures of serine β-lactamases have been solved in complex with AVI, supporting these mechanistic characteristics (3, 4, 8–10). Among class A β-lactamases, the strains producing CTX-M enzymes have proved to be successfully inhibited by the ceftazidime (CAZ)-avibactam combination (11).

The CTX-Ms are the most prevalent group of extended-spectrum β-lactamases (ESBLs) among pathogens around the world, which represent a global pandemic (12–14). CTX-Ms are generally more efficient in their ability to hydrolyze cefotaxime (CTX) and ceftriaxone (CRO) than ceftazidime (CAZ), although the spectrum varies by enzyme (15). This behavior was shown to be the consequence of a more favorable positioning of CTX in the active site for catalysis, which associated with disruption of a hydrogen bond between Asn170 and Asp240 (16). At this time, at least 230 unique CTX-M alleles are recognized, including both plasmid-encoded and chromosomal variants in *Kluyvera* species (17), which are distributed in at least five gene clusters with less than 5% amino acid sequence differences within each group (Beta-Lactamase DataBase [http://bldb.eu/]) (18).

An ESBL assigned as CTX-M-151 was recently isolated from a *Salmonella enterica* subsp. *enterica* serovar Choleraesuis TUM12370 strain in Japan (GenBank accession number NG_048937.1). In this study, we provide the kinetic characterization of this β-lactamase, along with structural evidence for the inhibition by AVI, and evaluate its phylogenetic relationship with the rest of the CTX-M family.

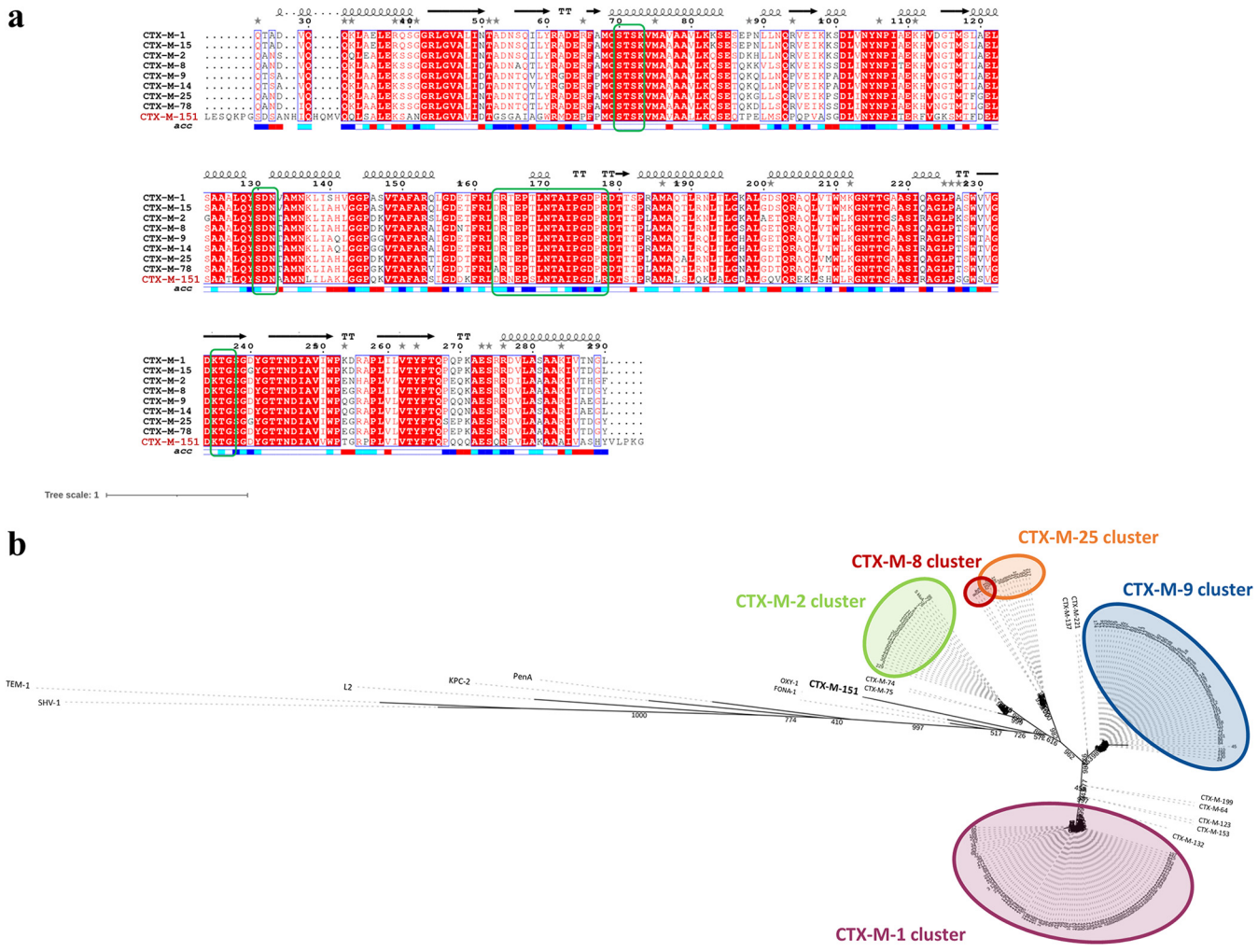

FIG 2 (a) Multiple alignment of amino acid sequences of CTX-M-151 and representative members from the five clusters of CTX-M β-lactamases, using the class A standard numbering scheme. Only the conserved motifs of the sequences are shown in green boxes for easier visualization. Locations of α-helices and β-sheets are indicated on the upper side (taken from the PDB file) and relative solvent accessibility on the bottom (blue, highly accessible; cyan, poorly accessible; white, hidden or nonaccessible). (b) Comparative phylogenetic tree constructed using all the nonredundant CTX-M β-lactamase sequences in June 2020, compared to selected enzymes from other class A families. Condensed clusters are shown in different colors for easier visualization of the lack of phylogenetic relationship of CTX-M-151 with the rest of the CTX-Ms.

RESULTS AND DISCUSSION

Sequence alignment of CTX-M-151. The deduced amino acid sequence of the β-lactamase from strain TUM12370, deposited as CTX-M-151 (GenBank accession number BAP34782.1), contains 304 residues. The predicted Sec-type signal peptide covers the first 23 residues (likelihood, 0.9961) (19), leaving a mature 281-amino-acid β-lactamase.

This mature protein possessed the highest identity with members from the CTX-M-9 subgroup. i.e., 68.9% and 69.3% identity with CTX-M-9 and CTX-M-14, respectively. Similar identity values were observed with some variants, such as CTX-M-64 and CTX-M-199, among others (20–22), and slightly lower values were observed with members of the CTX-M-1 (63.2% with CTX-M-15), CTX-M-2 (65%), CTX-M-8 (67.7%), and CTX-M-25 (66.9%) groups. Sequence alignment revealed the presence of "patches" of conserved residues, including those relevant for active site architecture (Fig. 2a). We note that this variant was originally annotated as a "CTX-M-9-like" enzyme within the Beta-Lactamase DataBase (BLDB [http://bldb.eu/BLDB.php?prot=A#CTX-M]) (18).

A comparative phylogenetic analysis revealed that CTX-M-151, despite its amino acid differences compared to the rest of the CTX-M family (Fig. 2b), remains more closely

TABLE 1 MICs against the source strain *S. Choleraesuis* and derived *E. coli* clones expressing $bla_{CTX\text{-}M\text{-}151}$

Drug	MIC (μg/ml) against:			
	E. coli BL21	*E. coli* BL21 + pET28	*E. coli* BL21 + pET28/$bla_{CTX\text{-}M\text{-}151}$	*S. Choleraesuis* TUM12370[a]
Ampicillin	0.5	0.25	2	128
Cephalothin	0.5	0.5	>128	>256
Cefoxitin	0.5	0.5	0.5	128
Ceftriaxone	≤0.125	≤0.125	64	8
Ceftazidime	0.5	0.5	0.5	8
Ceftazidime-avibactam	≤0.125	≤0.125	≤0.125	ND
Cefepime	≤0.125	≤0.125	8	1
Aztreonam	≤0.125	≤0.125	0.5	2
Imipenem	≤0.125	≤0.125	≤0.125	0.125

[a]Values from A. Yoshizumi and Y. Ishii (personal communication). ND, not determined.

related to the CTX-M family (and also to the FONA and OXY enzymes) than to other class A β-lactamases like TEM/SHV (~40% identity) or KPC (~50% identity), among others.

We stress that the sequence deposited in GenBank (accession number AB916359.1) shows that the genes immediately upstream and downstream of the *bla* gene encode a transcription elongation factor, GreB, and a putative L-lactate dehydrogenase operon regulatory protein, respectively. Although these neighboring genes are probable chromosomal genes, they are different from the genetic features commonly found associated with chromosomal $bla_{CTX\text{-}M/KLU}$ genes in *Kluyvera* species, i.e., an aspartate amino transferase gene located upstream of the $bla_{CTX\text{-}M/KLU}$ gene (replaced by an IS*Ecp1* or an IS*CR* element in plasmid-borne $bla_{CTX\text{-}M}$ genes), or either open reading frame 3 (orf3) or orf477 at the downstream region (17, 23).

These combined features suggest that this variant could either represent a new subfamily within the CTX-M β-lactamases or a new family of class A enzymes closely related to the CTX-M family. This differentiation will depend on the finding and analysis of further alleles in different isolates. Important questions remain as to the origin of this novel allele and the mechanism by which this β-lactamase evolved.

Antimicrobial susceptibility testing. Among the antibiotics tested, the $bla_{CTX\text{-}M\text{-}151}$ gene cloned into a pET vector, upon induction with isopropyl-β-D-thiogalactopyranoside (IPTG), conferred resistance to only cephalothin and ceftriaxone (CRO) when expressed in *Escherichia coli* BL21, and remained susceptible dose dependent (SDD) to cefepime (when applying the Clinical and Laboratory Standards Institute [CLSI] breakpoints). Susceptibility to ceftazidime (CAZ) agrees with the behavior of other "cefotaximases," like the CTX-Ms (Table 1). In the source *S.* Choleraesuis strain TUM12370, resistance to ampicillin, cephalothin, cefoxitin, and CRO was observed, while the isolate remained intermediate to CAZ and susceptible to aztreonam, cefepime, and imipenem. Also, AVI inhibited CTX-M-151 in *E. coli* clones when combined with CAZ.

Biochemical activity of CTX-M-151 reveals a substrate preference for CRO at the expense of diminished CAZ and penicillin hydrolytic activity. The principal steady-state kinetic parameters of CTX-M-151 are shown in Table 2. As expected, overall greater hydrolytic activity was observed against cephalosporins compared to the tested penicillins.

The activity toward CRO was at least 6,000-fold greater than toward for CAZ (k_{cat}/K_m, 0.6 versus 0.0001 $\mu M^{-1} \cdot s^{-1}$ for CRO and CAZ, respectively), which resembles the behavior of most of the CTX-M ESBLs. Regarding CAZ, the low k_{cat}/K_m value was mainly due to an elevated K_m value (in the millimolar range), and a very low k_{cat} value. The poor "ceftazidimase" activity was consistent with susceptibility to CAZ of the parent clones even after being induced (see Table 1).

Regarding penicillins, activity of CTX-M-151 was greater for piperacillin than ampicillin and benzylpenicillin (catalytic efficiencies were 0.79, 0.33, and 0.26 $\mu M^{-1} \cdot s^{-1}$, respectively), due to high K_m (234 μM for ampicillin) and low k_{cat} (12 s^{-1} for

TABLE 2 Steady-state kinetic parameters and standard deviations (SD) for CTX-M-151

Substrate	K_m (μM)	K_{cat} (s^{-1})	K_{cat}/K_m ($\mu M^{-1} \cdot s^{-1}$)	Relative k_{cat}/K_m (%)[a]
Nitrocefin	16 ± 2	170 ± 5	10.6 ± 1.6	
Benzyl-penicillin	47 ± 8	12.2 ± 0.6	0.26 ± 0.06	15.3
Ampicillin	234 ± 41	78 ± 6	0.33 ± 0.08	19.4
Piperacillin[b]	14 ± 1	11 ± 1	0.79 ± 0.08	46.5
Cephalothin	240 ± 28	409 ± 33	1.70 ± 0.34	100
Ceftriaxone	23 ± 3	13.3 ± 0.8	0.6 ± 0.1	35.3
Ceftazidime[b]	1,400 ± 60	0.14	0.0001 ± 0.000001	0.006
Cefepime	252 ± 75	200 ± 40	0.79 ± 0.23	46.5
Aztreonam	133 ± 24	66 ± 4	0.5 ± 0.1	29.4
Imipenem[b]	13 ± 1	0.001 ± 0.0001	0.00008 ± 0.00001	0.005

[a]Relative to cephalothin.
[b]The K_m values were determined as K_i in competition experiments against nitrocefin as reporter substrate (see Materials and Methods for further details).

benzylpenicillin) parameters. The "penicillinase" activity of this variant seemed to be up to 10-fold less than those of other CTX-M β-lactamases (24, 25).

Surprisingly, CTX-M-151 also demonstrated robust catalytic activity against aztreonam (k_{cat}/K_m = 0.79 $\mu M^{-1} \cdot s^{-1}$), in spite of the low MIC values observed both in the source *S. Choleraesuis* isolate and the transformant *E. coli* BL21 151-3 strain (Table 1). Additionally, we observed very poor activity toward imipenem, mostly due to a very low k_{cat} value (0.001 s^{-1}). Activity was not detected against cefoxitin (data not shown), for which a high MIC value was observed in the *S.* Choleraesuis isolate, indicating that additional resistance mechanisms are likely contributing.

Inhibition of CTX-M-151 by clavulanate and AVI. As expected for a class A β-lactamase, CTX-M-151 was well inhibited by clavulanate, with the following parameters: inhibition constant (K_i) of 0.17 ± 0.03 μM, inactivation rate (k_{inact}) of 0.026 ± 0.001 s^{-1}, and inhibition efficiency (k_{inact}/K_i) of 0.15 ± 0.03 $\mu M^{-1} \cdot s^{-1}$. These values were comparable to the values observed for other ESBLs like CTX-M-96 (0.67 μM, 0.03 s^{-1} and 0.045 $\mu M^{-1} \cdot s^{-1}$, respectively) (25) and PER-2 (0.064 μM, 0.031 s^{-1} and 0.48 $\mu M^{-1} \cdot s^{-1}$, respectively) (26).

The apparent inhibition constant ($K_{i\ app}$) for AVI determined by plotting $1/v_0$ versus [AVI] was found to be 0.4 μM (Table 3); this value is in the same range as that corresponding to KPC-2 (2) but 50-fold lower than that for PER-2 β-lactamase (27). In contrast, the $K_{i\ app}$ value obtained for CTX-M-151 was 10-fold greater than the value reported for wild-type SHV-1 (28). The acylation rate, k_2/K, was determined in our assays to be 37,000 $M^{-1} \cdot s^{-1}$ (Table 3). Comparative analysis with other serine β-lactamases revealed that CTX-M-151 displayed similar acylation constants to those of class A KPC-2 and SHV-1 (2, 6) and class C CMY-2 (28), with k_2/K values in the 10^4 $M^{-1} \cdot s^{-1}$ order (1.7×10^4 to 6×10^4 $M^{-1} \cdot s^{-1}$). These values are between 2 and 7.5-fold lower than k_2/K values for other class A β-lactamases, such as TEM-1 and CTX-M-15 (6, 13), but ~10-fold higher than those for class D OXA-48 (2).

TABLE 3 Comparative enzyme inhibition kinetic parameters and standard deviations (SD) of CTX-M-151 and other serine β-lactamases against AVI

β-Lactamase	$K_{i\ app}$ (μM)	k_2/K ($M^{-1} \cdot s^{-1}$)	K_{off} (s^{-1})	Reference or source
CTX-M-151	0.4 ± 0.03	$3.7 \times 10^4 \pm 0.1 \times 10^4$	$1.5 \times 10^{-3} \pm 0.1 \times 10^{-3}$	This study
CTX-M-15		$1.3 \times 10^5 \pm 0.1 \times 10^5$	$3 \times 10^{-4} \pm 1 \times 10^{-4}$	2
PER-2	20 ± 3	$2.2 \times 10^3 \pm 0.1 \times 10^3$	4×10^{-4}	10
KPC-2	1.2 ± 0.1	$1.3 \times 10^4 \pm 0.1 \times 10^4$	$1.4 \times 10^{-4} \pm 0.1 \times 10^{-4}$	2
SHV-1	0.022 ± 0.002	6×10^4		6
TEM-1		$1.6 \times 10^5 \pm 0.1 \times 10^5$	$8 \times 10^{-4} \pm 4 \times 10^{-4}$	1
OXA-48		$1.4 \times 10^3 \pm 0.1 \times 10^3$	$1.2 \times 10^{-5} \pm 0.4 \times 10^{-5}$	2
CMY-2	26 ± 3	$4.9 \times 10^4 \pm 0.5 \times 10^4$	$3.7 \times 10^{-4} \pm 0.4 \times 10^{-4}$	28

TABLE 4 X-ray data collection and refinement statistics

Parameter	Crystal	
	Apo CTX-M-151	CTX-M-151/AVI
PDB code	6BN3	6BPF
Data collection		
No. of frames	3,600	3,600
Oscillation step (°)	0.1	0.1
Detector distance (mm)	126.96	134.26
Wavelength (Å)	0.9801	0.9801
Exposure per frame (s)	0.025	0.025
Space group	*C* 2	*C* 2
Unit cell parameters (Å [°])	a = 95.79, b = 41.81, c = 56.45 (α = 90, β = 94.14, γ = 90)	a = 95.59, b = 41.94, c = 56.36 (α = 90, β = 94.09, γ = 90)
No. of subunits/asymmetric units	1	1
Resolution range (Å)[a]	47.77–1.28 (1.32–1.28)	47.67–1.32 (1.40–1.32)
Total no. of reflections	370,005	337,693
No. of unique reflections	56,860 (5,258)	52,411 (8,155)
Redundancy	6.5 (5.9)	6.4 (5.7)
Completeness (%)	98.1 (91.4)	99.2 (96.1)
Mean I/σ (I)	12.5 (1.4)	14.3 (1.3)
Overall Wilson *B* factor (Å^2)	18	18
R_{merge}	0.066 (0.847)	0.065 (0.833)
R_{meas}	0.072 (0.929)	0.071 (0.919)
CC (1/2)	0.998 (0.834)	0.999 (0.838)
Refinement		
No. of reflections used in refinement	56,738	52,272
R_{free} test set (%)	2,839 (5.0)	2,615 (5.0)
R_{work}	0.166	0.188
R_{free}	0.214	0.213
No. of nonhydrogen atoms	2,309	2,318
No. of macromolecules	2,021	1,986
No. of ligands	15	17
No. of solvents	273	315
RMS[b] deviations from ideal stereochemistry		
Bonds (Å)	0.006	0.008
Angles (°)	1.11	1.03
Avg *B* factor (Å^2)		
All atoms	25	22
Protein	24	21
Ligand	44	18
Solvent	35	32
Ramachandran plot (%)		
Favored regions	97.4	96.9
Allowed regions	2.3	2.7
Outlier regions	0.3	0.4

[a]Statistics for the highest-resolution shell are given in parentheses.
[b]RMS, root mean square.

Recovery of CTX-M-151 activity after inhibition by AVI was measured next. The deacylation rate, k_{off}, was found to be 0.0015 s^{-1} (Table 3). Interestingly, the off-rate (k_{off}) for CTX-M-151 was between 2- and 14-fold greater than those for other class A β-lactamases, with the carbapenemase KPC-2 being the lowest among these enzymes. Comparing other enzymes, we observed a 125-fold greater rate than that of the carbapenem-hydrolyzing class D β-lactamase (CHDL) OXA-48 and a 4-fold greater rate than that of the class C β-lactamase CMY-2.

Crystallographic structure of apo-CTX-M-151 and its complex with AVI. The structure of the apo form of CTX-M-151 and its covalent complex with AVI were obtained at resolutions of 1.28 and 1.32 Å, respectively. Data collection and refinement

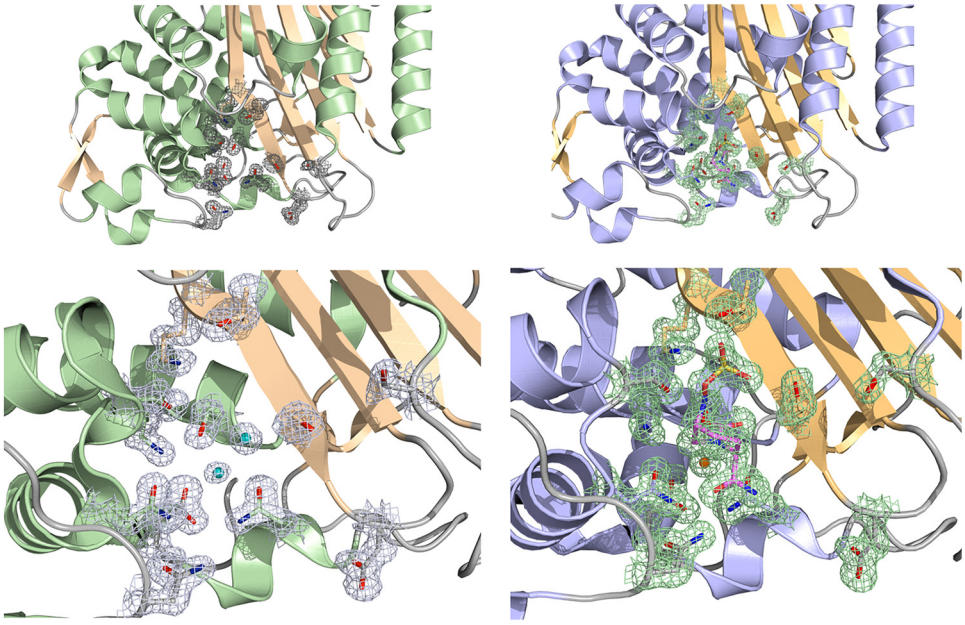

FIG 3 (Upper) Overall structures of the apo CTX-M-151 (green/orange) and its complex with AVI (purple/orange). (Lower) Detail of the active site of apo CTX-M-151 (left) and the CTX-M-151/AVI complex (right). Important residues and the AVI molecule are shown surrounded by the corresponding electron density maps contoured at the 2.5-σ level (gray for the apo form and green for the complex) for better visualization. Also, the conserved water molecules are shown as turquoise (apo enzyme) or orange (complex) spheres; note that in the CTX-M-151/AVI complex, only the deacylation water is found.

statistics are given in Table 4. Both structures contained only one monomer per asymmetric unit, and the electron density map was well defined along the main chain in both cases (Fig. 3). The protein chains for apo CTX-M-151 and the CTX-M-151/AVI complex include 267 and 265 residues, respectively. The structures were solvated by 273 (apo form) and 315 (AVI complex) ordered water molecules. The average root mean square deviation (RMSD) values for alpha carbon (C-α) atoms between the main chains of CTX-M-151 and its complex with AVI was 0.16 Å.

Inspection of the CTX-M-151/AVI complex revealed that AVI was covalently bound to the Ser70-O$^{\gamma}$ atom upon cleavage of the C-7–N-6 bond, excluding the possibility of cleavage of the C-7–N-1 bond, in agreement with other structures with bound AVI (9, 10). This was clearly observed in the active site in the well-defined mF_o-DF_c omit map contoured at the 2.5-σ level for the AVI moiety (Fig. 4a). The 6-membered AVI ring adopted a chair conformation with hydrogen bonds via the C-7 carbonyl of the newly formed carbamate (which occupied the place of the catalytic water in the apo structure, as observed in Fig. 4b and c) to the backbone nitrogen atoms of Ser70 and Ser237 in the oxyanion hole, and to the carbonyl oxygen atom of Ser237 (2.65, 2.92, and 3.07 Å, respectively; Fig. 4a). Additional hydrogen bond interactions were observed (i) between the C-2 amide oxygen atom of AVI and Asn132-N$^{\delta 2}$ (2.72 Å), (ii) between the amide nitrogen atom with two water molecules, (iii) between AVI-N6 with Ser130-O$^{\gamma}$ (2.94 Å), (iv) via the AVI sulfate moiety with Thr235-O, Thr235-O$^{\gamma}$, Ser237-O$^{\gamma}$, and (v) between two additional water molecules. Further interactions contributing to the proper fitting of AVI occurred in the active site, creating second-shell hydrogen bonds, and included Asn104 and Lys73 (through Asn132), Thr216 (through Thr235), and several water molecules. The spatial position of the AVI sulfate moiety, equivalent to that for the β-lactam carboxylate group, was occupied, oddly, by a HEPES molecule in the apo CTX-M-151 structure (data not shown).

Upon binding of AVI, the deacylating water was slightly displaced outwards Ser70-O$^{\gamma}$ in comparison to its position in the apo form (2.88 versus 2.59 Å) so that the side

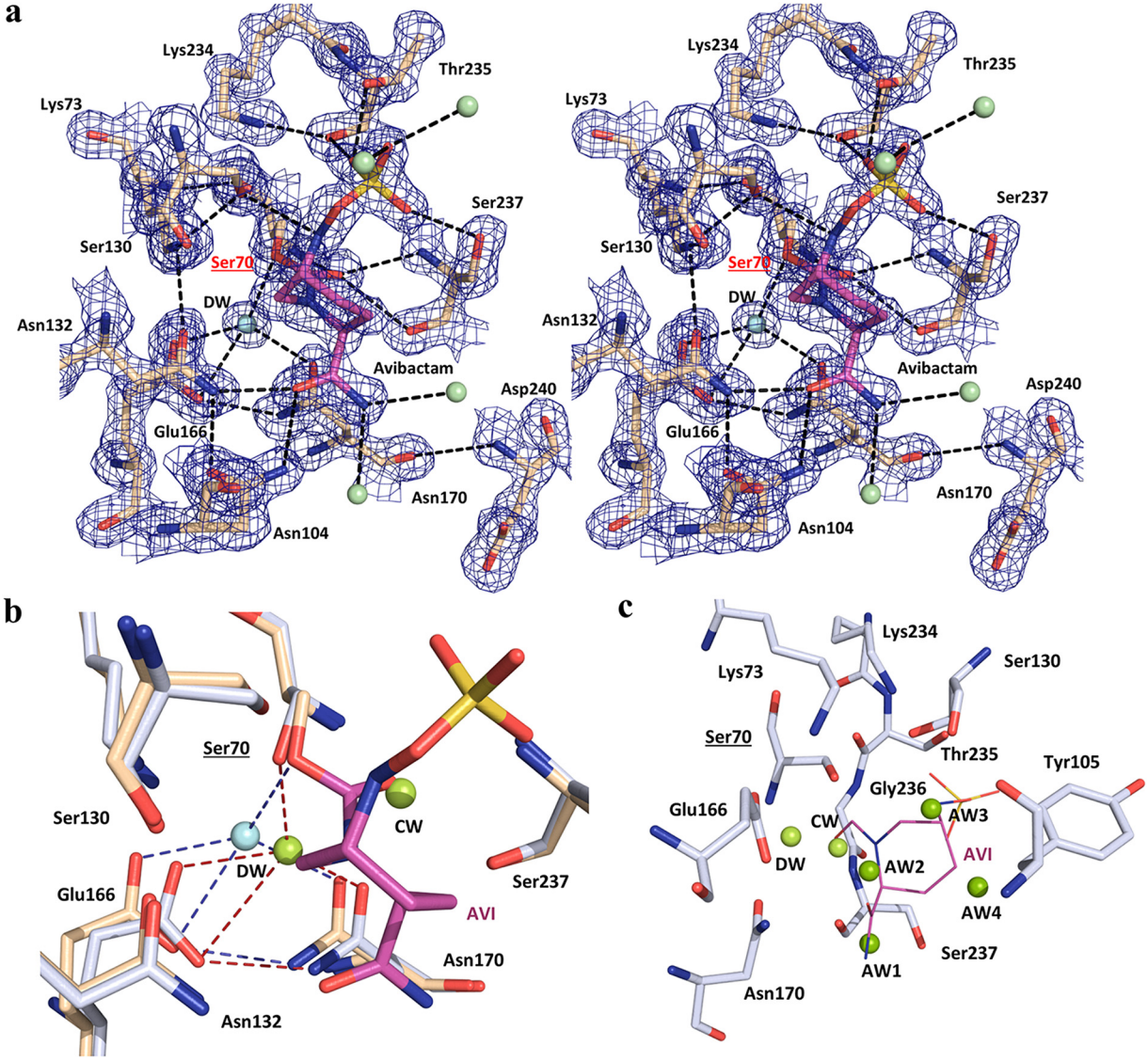

FIG 4 (a) Stereo view of the CTX-M-151/AVI complex showing the main hydrogen bond interactions in the active site (black dashed lines). The $2mF_o$-DF_c map is contoured at the 1.5-σ level (blue). Water molecules are shown as spheres with different colors, depending on their function, with deacylating water (DW) in cyan and other important molecules participating in AVI stabilization in green. The relevant Ser70 residue is highlighted in red. (b) Comparative stabilization of the hydrogen bond network (dashed lines) in apo CTX-M-151 (light blue) and the AVI complex (light orange) and displacement of the deacylating water (DW) upon AVI binding. CW, catalytic water. (c) Position of additional water molecules (AW) replaced by the piperidine ring and amide moieties when AVI is bound to Ser70, presumably creating a conserved hydrogen bonding network in apo CTX-M-151.

chains of Glu166 and Asn170 were shifted to create the proper hydrogen bonding network (Fig. 4b). Also, the positions of several water molecules seem to have been replaced by the piperidine ring and amide moieties of the AVI molecule, which could presumably take part in a conserved hydrogen bonding network in apo CTX-M-151 (Fig. 4c). In fact, this could give rise to a more favorable environment for creating hydrophobic interactions between Tyr105 and the 6-membered AVI ring.

More importantly, we observed a subtle yet evident functional difference between the apo and complex structures, which was also observed in the CTX-M-15/AVI structure. In the CTX-M-151/AVI complex, the side chain of Lys73 points toward Ser130 (in the apo structure, Lys73 is oriented toward Glu166 and Ser70 instead), which was associated with the protonation of Glu166, observable due to the high resolution of the structure (Fig. 5), and relevant in the orientation and activation of the deacylating

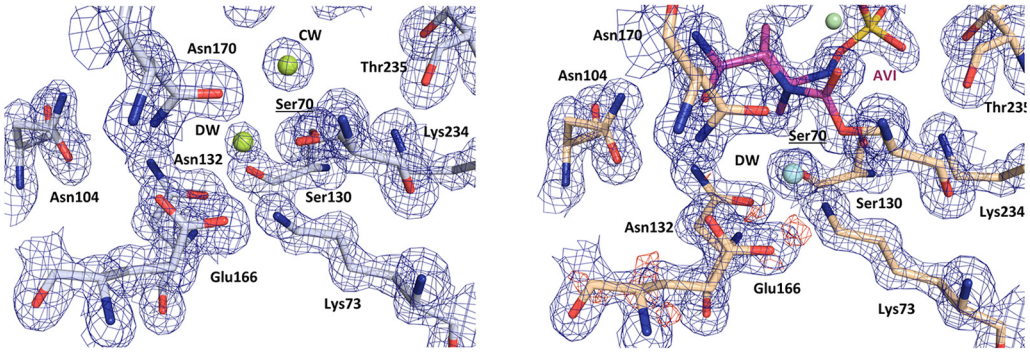

FIG 5 Differences in the orientation of Lys73 in the apo (left) and CTX-M-151/AVI complex (right) structures (see the text for details). The $2mF_0$-DF_c map (contoured at 1.5 σ) is shown in blue, and the mF_0-DF_c map (contoured at 3 σ) is shown in red.

water during catalysis (9). These observations would support the role of Lys73 in the proton relay pathway in β-lactam catalysis (29) and Glu166 as the general base in deacylation (30, 31).

Comparative interaction of AVI with CTX-M-151 and other class A β-lactamases. When the CTX-M-151/AVI complex structure was compared by superposition to other class A β-lactamases, the RMSD values (in Å) for the C-α atoms between the main chain of CTX-M-151 and other class A β-lactamases were 0.57 (CTX-M-15), 1.45 (SHV-1), 1.06 (KPC-2), 1.03 (L2), 1.06 (VCC-1), and 1.70 (PER-2). Also, the position and spatial arrangement of AVI within the active site was conserved overall in all compared structures (Fig. 6a).

Although the degree of sequence similarity between CTX-M-151 and CTX-M-15 (or other members within the family) was much lower (70%) than those between each of the other CTX-M enzymes (>90%), a high conservation in the position of the catalytically relevant residues, accompanied by a tight conformational stability of the active site, was noted. The only difference in the interaction between AVI and both enzymes was the absence of a hydrogen bond between the sulfate moiety of AVI and Ser237 in CTX-M-15 (separated by 3.39 Å), and the presence of a direct hydrogen bond between the carbonyl oxygen of the AVI carboxamide group and Asn104-$N^{\delta 2}$ (Fig. 6b).

The mechanisms of AVI inhibition. Debate is still present regarding the mechanism by which class A β-lactamases are inhibited by AVI. The consensus is that the catalytic Ser70 residue is primed for the nucleophilic attack on the electrophilic C-7 carbonyl carbon atom of AVI creating a high-energy tetrahedral intermediate that results in a carbamoyl enzyme intermediate.

We observed a possible protonation of Glu166 upon AVI binding, associated with a shift in the position of Lys73 away from Glu166 and toward Ser130 (Fig. 5). This finding agrees with previous observations in CTX-M-15/AVI (9) and the proposed mechanism involving a proton shuttle from Lys73 to Ser130 in CTX-M β-lactamases (32). Moreover, noting that Glu166 is deprotonated in the apo CTX-M-151 structure, and therefore charged, converts this residue as the most probable general base in the priming of Ser70 during the acylation step of AVI inhibition.

Conclusions. Using genetic, microbiological, biochemical, and structural tools, we characterized CTX-M-151, a novel enzyme with the lowest degree of similarity within the CTX-M family. Both the low relative percent identity compared to the rest of the CTX-M members and its phylogenetic divergence from the five compact clusters within the family prompted us to suggest that this variant may represent a new subgroup within the family. It is also possible that this enzyme might represent a new group of β-lactamases that are closely related to the CTX-Ms. At this point in time, further studies are required to understand the place of this β-lactamase in the class A group of enzymes. Additionally, insights into the structure of CTX-M-151 in complex with AVI

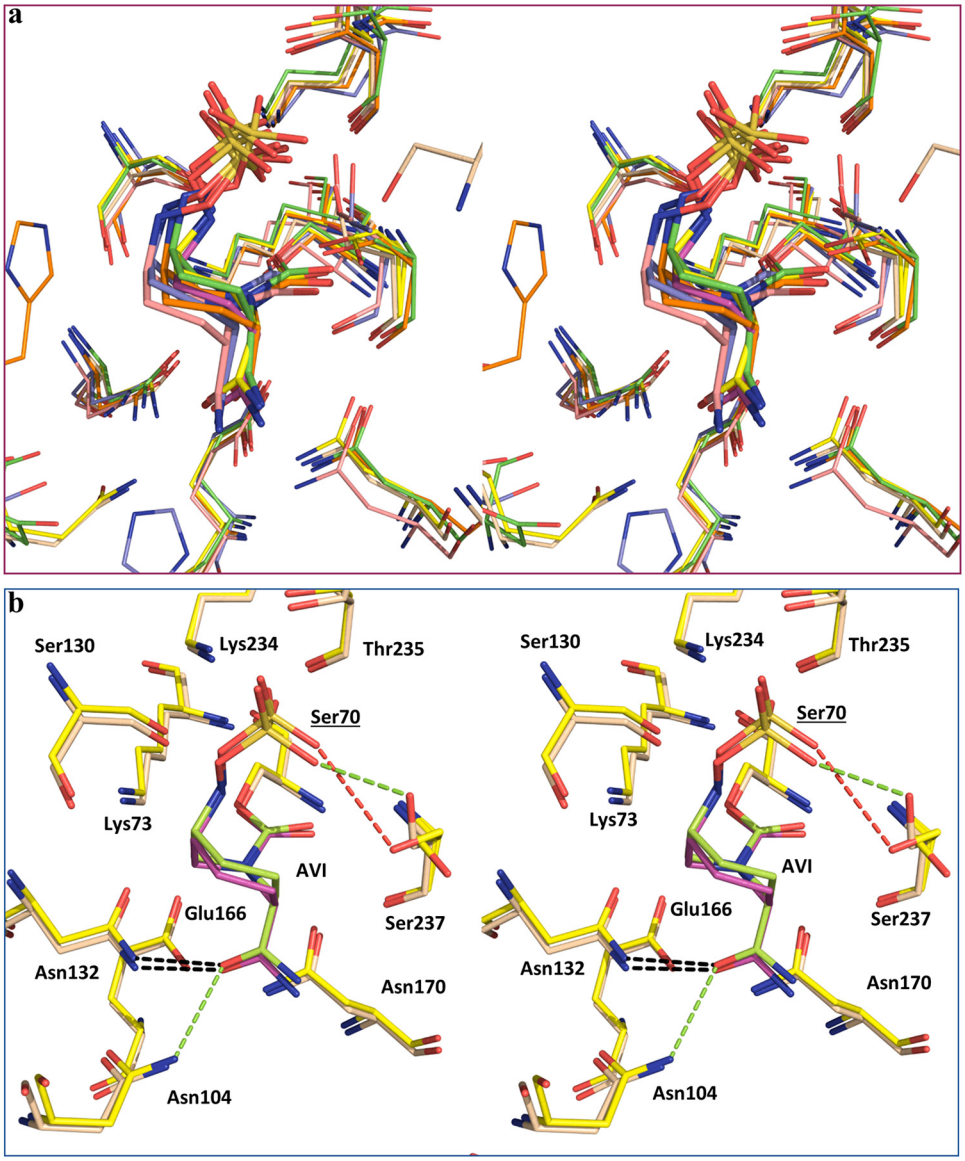

FIG 6 (a) Overlay positioning of AVI in the active site of different class A β-lactamases (stereo view). CTX-M-151 (light orange/magenta), CTX-M-15 (yellow), KPC-2 (pink), SHV-1 (green), PER-2 (blue), L2 (orange). (b) Stereo view showing the differences in the interaction of AVI in the active site of CTX-M-151 (light orange/magenta) and CTX-M-15 (yellow/green). Common hydrogen bonds are shown as black dashed lines, whereas differential interactions are shown in green. Red lines denote interactions that are missing due to a long distance between the atoms involved (see the text for details).

revealed similar interactions of the inhibitor with residues in the active site of this singular ESBL, which support the efficacy of AVI toward a wide range of serine β-lactamases.

To our knowledge, this is the first ESBL found chromosomally encoded in *S.* Choleraesuis. It is noteworthy that most of the chromosomally encoded ESBLs found in *Enterobacterales* species show similar catalytic features, with hydrolytic preference toward CTX/CRO compared to CAZ, i.e., CTX-M (*Kluyvera* spp.) (17, 33–35), FONA (*Serratia fonticola*) (36), OXY (*Klebsiella oxytoca*) (37), RAHN (*Rahnella aquatilis*) (38), SFO (*Enterobacter cloacae*) (39), and SMO (*Ewingella* sp.) (40). It is interesting to observe that different enterobacterial species offer a portfolio of β-lactamases having equivalent hydrolytic profiles. Whether the low efficiency in hydrolyzing CAZ compared to other oxyimino-cephalosporins is a mere coincidence or is connected to other structural properties of these enzymes (e.g., lower stability) remains to be further explored.

Experiments are under way to attempt to understand this important phenomenon, as well as the place of this novel variant among other resistance determinants.

MATERIALS AND METHODS

Bacterial strains and plasmids. The $bla_{CTX\text{-}M\text{-}151}$ gene was recovered from a *S.* Choleraesuis TUM12370 strain isolated from a piglet's feces in Tokyo, Japan, in 2014. *E. coli* ATCC 25922 was used for quality control in antimicrobial susceptibility assays. *E. coli* DH5α (Invitrogen, USA) and *E. coli* BL21(DE3) (Novagen, USA) were hosts for transformation experiments. Plasmid vectors pGEM-T easy vector (Promega, USA) and kanamycin-resistant pET28a(+) (Novagen, Germany) were employed for routine cloning experiments and for β-lactamase purification, respectively.

Chemical compounds. Avibactam (AVI) was acquired through an investigator-initiated trial with Allergan. Ampicillin (AMP), aztreonam (ATM), cefepime (FEP), ceftazidime (CAZ), ceftriaxone (CRO), cefoxitin (FOX), cephalothin (CEF), imipenem (IPM), and piperacillin (PIP) were obtained from Klonal (Argentina). Nitrocefin (NCF) was purchased from Becton, Dickinson and from Oxoid.

Antimicrobial susceptibility testing. MICs were obtained by the broth microdilution method according to the CLSI guidelines (41). AVI was used at a fixed concentration (4 μg/ml) when combined with CAZ. For recombinant *E. coli* BL21 clones expressing CTX-M-151, Mueller-Hinton broth was supplemented with 1 mM IPTG, and MIC was determined as above upon incubation at 37°C for 16 to 20 h.

Recombinant DNA methods. The $bla_{CTX\text{-}M\text{-}151}$ gene was amplified by PCR from a recombinant *E. coli* clone harboring the pET9a/blaCTX-M-151 plasmid (provided by Y. Ishii), using Phusion high-fidelity DNA polymerase (Thermo Scientific, USA). Two PCR products were obtained using primers 151-Nco-F1-i.e., (5′-CCATGGTCAATAAACGGCTGAGTATTGCTC-3′) and 151-BamH-R1 (5′-GGATCCTCAGCCTTTAGGCAATAC ATAATGG-3′) for the complete coding sequence (CDS) of $bla_{CTX\text{-}M\text{-}151}$ and 151-Nde-F2-ht (5′-CATATGG CCCYCGAGAGCCAGAAG-3′) and 151-BamH-R1 for the sequence encoding the mature CTX-M-151. The PCR products were first cloned in a pTZ57R/T vector, and the insert was sequenced for verification of the identity of the $bla_{CTX\text{-}M\text{-}151}$ gene and generated restriction sites, as well as the absence of aberrant nucleotides. Resulting recombinant pTZ57R/T plasmids were then digested, and the released inserts cloned in a pET28a (+) vector. Ligation mixtures were used to first transform *E. coli* DH5α competent cells, and selected recombinant clones were sequenced to confirm the identity of the $bla_{CTX\text{-}M\text{-}151}$ gene. Then, those clones harboring the resulting pET plasmids were used for a second transformation step in *E. coli* BL21(DE3) competent cells. *E. coli* carrying the full-length $bla_{CTX\text{-}M\text{-}151}$ gene was used to determine the MICs, whereas *E. coli* expressing the mature form of CTX-M-151 was used for protein expression and purification.

DNA sequencing and bioinformatics. DNA sequences were determined at Macrogen, Inc. (South Korea). Nucleotide and amino acid sequence analyses were conducted using NCBI (http://www.ncbi.nlm.nih.gov/) and ExPASy (http://www.expasy.org/) analysis tools. Sequence and structural alignments were also performed using T-Coffee Expresso (42) and ESPript/ENDscript (43). For the phylogenetic tree, 222 $bla_{CTX\text{-}M}$ nonredundant nucleotide sequences were downloaded from the GenBank database (http://www.ncbi.nlm.nih.gov) in June 2020. The corresponding nucleotide sequences were aligned using ClustalW, and the alignment was manually revised and modified where necessary. The maximum likelihood phylogenetic tree of the revised alignment was obtained using the PhYML web server. Evolutionary model selection was conducted using the Smart Model Selection (SMS) tool integrated into the PhYML web server, and the Bayesian information criterion (BIC) was chosen as the selection criterion (44, 45). The robustness of the relevant nodes was estimated with 1,000 bootstrap replicates.

Expression and purification of CTX-M-151. An overnight culture of recombinant *E. coli* BL21 producing CTX-M-151 was diluted (1/20) in 500 ml lysogeny broth (LB) containing 30 μg/ml kanamycin and grown at 37°C until ca. 0.9 optical density (OD) units (λ = 600 nm). To induce β-lactamase expression, 1 mM IPTG was added. After 20 h of further incubation at 28°C, crude extracts were obtained through ultrasonic disruption, and after clarification by centrifugation at 10,000 $\times$ *g* for 20 min (4°C; Sorvall GS3 rotor), clear supernatants containing CTX-M-151 were dialyzed overnight against 2.5 liters of buffer A (50 mM Tris and 200 mM NaCl [pH 8.0]). Clear supernatants were filtered by 0.45-μm-pore-size membranes and loaded onto a 5-ml HisTrap high-performance (HP) column (GE Healthcare Life Sciences, USA), connected to an Äkta purifier (GE Healthcare Life Sciences, USA) and preequilibrated with buffer A. The column was extensively washed to remove unbound proteins, and β-lactamases were eluted with a linear gradient (0 to 100%; 2 ml/min flow rate) of buffer B (50 mM Tris, 200 mM NaCl, and 500 mM imidazole [pH 8.0]). Eluted fractions were screened *in situ* for β-lactamase activity during purification by NCF hydrolysis and confirmed by SDS-PAGE in 12% polyacrylamide gels. Thrombin digestion (GE Healthcare Life Sciences) was performed overnight at 16°C to remove the histidine tag, according to the manufacturer's indications, and the tag was further removed by affinity chromatography in 1-ml HisTrap HP columns. Eluted proteins were conserved at −70°C until use. Protein concentration and purity were determined by UV absorbance at 280 nm (according to the Lambert-Beer law and molar extinction coefficient) and by Coomassie blue staining on 15% SDS-PAGE gels, respectively.

Kinetics. Steady-state kinetic parameters were determined using a T80 UV-visible spectrophotometer (PG Instruments, Ltd., UK). Each reaction was performed in triplicate in 25 mM phosphate buffer (pH 7.0) at 22°C. The steady-state kinetic parameters K_m and maximum rate of metabolism (V_{max}) were obtained as described previously (27, 46) with nonlinear least-squares fitting of the data (Henri Michaelis-Menten equation) using Prism 5.03 for Windows (GraphPad Software, San Diego, CA) according to Equation 1, as follows:

$$v = \frac{V_{\max} \times [S]}{K_m + [S]} \quad (1)$$

For high K_m values, the k_{cat} values were derived by evaluation of the complete hydrolysis time courses as described by De Meester et al. (47). For poor substrates behaving as competitive inhibitors, apparent K_m values were determined as K_i by monitoring the residual activity of the enzyme in the presence of various concentrations of the drug and 100 μM nitrocefin as the reporter substrate in competition experiments, according to the following expression (Equation 2):

$$v = V(S) / \left[(S) + K_m \left(1 + \frac{I}{K_i} \right) \right] \quad (2)$$

in which K_m and S correspond to the reporter substrate and I is the variable concentration for the competitive substrate.

For irreversible inhibitors (clavulanic acid), the rate constant of inactivation (k_{inact}) was measured directly by time-dependent inactivation of CTX-M-151 in the presence of the inhibitor, using a fixed concentration of enzyme and 100 μM NCF as a reporter and increasing concentrations of the inhibitor (concentration range, 0.055 to 1.1 μM). The observed rate constant for inactivation (k_{obs}) was determined by nonlinear least-squares fitting of the data using OriginPro 8.0 (Northampton, MA), using Equation 3, as described elsewhere (26, 48).

The interaction of CTX-M-151 with AVI was assumed to follow the models of other β-lactamases except that of KPC-2 (1), proposed by Ehmann (2), on the basis of the scheme shown in Fig. 1b, where K_i (k_{-1}/k_1) is the dissociation constant of the *EI* complex (also referred to as *K* in some references) (49, 50). The inhibition constants K_i and k_2/K were determined as reported previously for AVI in competitive assays using 110 μM NCF (as a reporter substrate) and increasing AVI concentrations (range, 0.024 to 1.6 μM) (27). Progress curves were subsequently fitted to Equation 3 to obtain k_{obs} values.

$$A = A_0 + v_f \times t + (v_0 - v_f) \times (1 - e^{-k_{obs} \times t}) / k_{obs} \quad (3)$$

Finally, k_{obs} values were plotted against [AVI], and the k_2/K value was obtained by correcting the value for the slope of the line for the concentration and affinity of NCF (Equation 4).

$$k_2/K_{corrected} = k_2/K_{obs} \times [([S]/K_{m\,nitrocefin}) + 1] \quad (4)$$

The k_{off} value was determined by incubating the CTX-M-151 with an AVI concentration that resulted in complete inhibition, as follows: 1 μM enzyme was preincubated with 120 μM AVI, samples were serially diluted (1:2,000), and hydrolysis of 100 μM NCF was measured. Progress curves were fitted to a single exponential decay equation as previously described (1, 27).

The following extinction coefficients and wavelengths were used (51): ampicillin ($\Delta\varepsilon_{235}$ = -820 $M^{-1} \cdot cm^{-1}$), cephalothin ($\Delta\varepsilon_{273}$ = $-6{,}300$ $M^{-1} \cdot cm^{-1}$), CAZ ($\Delta\varepsilon_{260}$ = $-9{,}000$ $M^{-1} \cdot cm^{-1}$), CRO ($\Delta\varepsilon_{260}$ = $-9{,}400$ $M^{-1} \cdot cm^{-1}$), cefepime ($\Delta\varepsilon_{260}$ = $-10{,}000$ $M^{-1} \cdot cm^{-1}$), aztreonam ($\Delta\varepsilon_{318}$ = -750 $M^{-1} \cdot cm^{-1}$), and nitrocefin ($\Delta\varepsilon_{482}$ = $+15{,}000$ $M^{-1} \cdot cm^{-1}$).

Crystallization of apo and AVI-bound CTX-M-151. Crystals of apo CTX-M-151 were grown by the hanging drop vapor diffusion method (20°C) with drops containing 2 μl of enzyme solution (20 mg/ml) and 2 μl of crystallization solution consisting of 21% (wt/vol) polyethylene glycol (PEG) 8,000 and 0.1 M HEPES (pH 7.8). The AVI adduct was obtained by soaking apo CTX-M-151 crystals in crystallization solution supplemented with 100 mM AVI for 24 h. All samples were cryoprotected in mother liquor with 15% (wt/vol) PEG 400 added and then flash-cooled in liquid nitrogen in Hampton Research loops (Aliso Viejo, USA).

Data collection, phasing, and model building and refinement. Native X-ray diffraction data were collected at 100 K at the Proxima 2A beamline at the Soleil Synchrotron (Saint Aubin, France), using a Dectris Eiger X 9M detector. Integration and scaling were carried out using XDS software (52). Structure resolution was achieved by molecular replacement through Phaser (53), using the CTX-M-14 structure (Protein Data Bank [PDB] code 4UA6) as a starting model (54). Refinement and model building were performed with Phenix 1.12-2829 (55) and Coot 0.8.6.1 (Turtle Bay) (56), respectively. Models were visualized with PyMOL 1.7.0.3 (57).

Accession number(s). The coordinates and structure factor amplitudes of apo CTX-M-151 and the CTX-M-151/AVI complex were deposited in the Protein Data Bank (PDB) under accession codes 6BN3 and 6BPF, respectively.

ACKNOWLEDGMENTS

This work was funded in part by grants from the University of Buenos Aires (UBACyT 2014-2017 to P.P.), Agencia Nacional de Promoción Científica y Tecnológica (BID PICT 2014-0457 to P.P. and PICT 2015-1925 to G.G.). Research reported in this publication was supported in part by the National Institute of Allergy and Infectious Diseases of the National Institutes of Health under award numbers R01AI100560, R01AI063517, and R01AI072219 to R.A.B. This study was supported in part by funds

and/or facilities provided by the Louis Stokes Cleveland VA Medical Center, award number 1I01BX002872 to K.M.P.-W., Biomedical Laboratory Research & Development Service of the VA Office of Research and Development award number 1I01BX001974 to R.A.B., and the Geriatric Research Education and Clinical Center VISN 10 program to R.A.B.

The content is solely the responsibility of the authors and does not necessarily represent the official views of the National Institutes of Health or the Department of Veterans Affairs.

We thank Allergan for providing the avibactam powder. We acknowledge access to the Proxima 2A beamline at the Soleil Synchrotron, France, and acknowledge the NCBI for support with the nomenclature definition.

P.P., B.G., M.M.R., S.K., and G.G. are researchers at the Consejo Nacional de Investigaciones Científicas y Técnicas (CONICET, Argentina).

REFERENCES

1. Ehmann DE, Jahic H, Ross PL, Gu RF, Hu J, Kern G, Walkup GK, Fisher SL. 2012. Avibactam is a covalent, reversible, non-β-lactam β-lactamase inhibitor. Proc Natl Acad Sci U S A 109:11663–11668. https://doi.org/10.1073/pnas.1205073109.
2. Ehmann DE, Jahic H, Ross PL, Gu RF, Hu J, Durand-Reville TF, Lahiri S, Thresher J, Livchak S, Gao N, Palmer T, Walkup GK, Fisher SL. 2013. Kinetics of avibactam inhibition against class A, C, and D β-lactamases. J Biol Chem 288:27960–27971. https://doi.org/10.1074/jbc.M113.485979.
3. Krishnan NP, Nguyen NQ, Papp-Wallace KM, Bonomo RA, van den Akker F. 2015. Inhibition of *Klebsiella* β-lactamases (SHV-1 and KPC-2) by avibactam: a structural study. PLoS One 10:e0136813. https://doi.org/10.1371/journal.pone.0136813.
4. Lahiri SD, Mangani S, Jahic H, Benvenuti M, Durand-Reville TF, De Luca F, Ehmann DE, Rossolini GM, Alm RA, Docquier JD. 2015. Molecular basis of selective inhibition and slow reversibility of avibactam against class D carbapenemases: a structure-guided study of OXA-24 and OXA-48. ACS Chem Biol 10:591–600. https://doi.org/10.1021/cb500703p.
5. Papp-Wallace KM, Winkler ML, Taracila MA, Bonomo RA. 2015. Variants of β-lactamase KPC-2 that are resistant to inhibition by avibactam. Antimicrob Agents Chemother 59:3710–3717. https://doi.org/10.1128/AAC.04406-14.
6. Winkler ML, Papp-Wallace KM, Taracila MA, Bonomo RA. 2015. Avibactam and inhibitor-resistant SHV β-lactamases. Antimicrob Agents Chemother 59:3700–3709. https://doi.org/10.1128/AAC.04405-14.
7. Drawz SM, Bonomo RA. 2010. Three decades of β-lactamase inhibitors. Clin Microbiol Rev 23:160–201. https://doi.org/10.1128/CMR.00037-09.
8. Lahiri SD, Johnstone MR, Ross PL, McLaughlin RE, Olivier NB, Alm RA. 2014. Avibactam and class C β-lactamases: mechanism of inhibition, conservation of the binding pocket, and implications for resistance. Antimicrob Agents Chemother 58:5704–5713. https://doi.org/10.1128/AAC.03057-14.
9. Lahiri SD, Mangani S, Durand-Reville T, Benvenuti M, De Luca F, Sanyal G, Docquier JD. 2013. Structural insight into potent broad-spectrum inhibition with reversible recyclization mechanism: avibactam in complex with CTX-M-15 and *Pseudomonas aeruginosa* AmpC β-lactamases. Antimicrob Agents Chemother 57:2496–2505. https://doi.org/10.1128/AAC.02247-12.
10. Ruggiero M, Papp-Wallace KM, Brunetti F, Barnes MD, Bonomo RA, Gutkind G, Klinke S, Power P. 2019. Structural insights into the inhibition of the extended-spectrum β-lactamase PER-2 by avibactam. Antimicrob Agents Chemother 63:e00487-19. https://doi.org/10.1128/AAC.00487-19.
11. Giani T, Cannatelli A, Di Pilato V, Testa R, Nichols WW, Rossolini GM. 2016. Inhibitory activity of avibactam against selected β-lactamases expressed in an isogenic *Escherichia coli* strain. Diagn Microbiol Infect Dis 86:83–85. https://doi.org/10.1016/j.diagmicrobio.2016.03.002.
12. Gutkind GO, Di Conza J, Power P, Radice M. 2013. β-Lactamase-mediated resistance: a biochemical, epidemiological and genetic overview. Curr Pharm Des 19:164–208. https://doi.org/10.2174/138161213804070320.
13. Rossolini GM, D'Andrea MM, Mugnaioli C. 2008. The spread of CTX-M-type extended-spectrum β-lactamases. Clin Microbiol Infect 14:33–41. https://doi.org/10.1111/j.1469-0691.2007.01867.x.
14. Canton R, Coque TM. 2006. The CTX-M β-lactamase pandemic. Curr Opin Microbiol 9:466–475. https://doi.org/10.1016/j.mib.2006.08.011.
15. Bush K, Bradford PA. 2020. Epidemiology of β-lactamase-producing pathogens. Clin Microbiol Rev 33:e00047-19. https://doi.org/10.1128/CMR.00047-19.
16. Delmas J, Leyssene D, Dubois D, Birck C, Vazeille E, Robin F, Bonnet R. 2010. Structural insights into substrate recognition and product expulsion in CTX-M enzymes. J Mol Biol 400:108–120. https://doi.org/10.1016/j.jmb.2010.04.062.
17. Rodriguez MM, Power P, Radice M, Vay C, Famiglietti A, Galleni M, Ayala JA, Gutkind G. 2004. Chromosome-encoded CTX-M-3 from *Kluyvera ascorbata*: a possible origin of plasmid-borne CTX-M-1-derived cefotaximases. Antimicrob Agents Chemother 48:4895–4897. https://doi.org/10.1128/AAC.48.12.4895-4897.2004.
18. Naas T, Oueslati S, Bonnin RA, Dabos ML, Zavala A, Dortet L, Retailleau P, Iorga BI. 2017. β-Lactamase DataBase (BLDB)—structure and function. J Enzyme Inhib Med Chem 32:917–919. https://doi.org/10.1080/14756366.2017.1344235.
19. Almagro Armenteros JJ, Tsirigos KD, Sonderby CK, Petersen TN, Winther O, Brunak S, von Heijne G, Nielsen H. 2019. SignalP 5.0 improves signal peptide predictions using deep neural networks. Nat Biotechnol 37:420–423. https://doi.org/10.1038/s41587-019-0036-z.
20. He D, Chiou J, Zeng Z, Chan EW, Liu JH, Chen S. 2016. Comparative characterization of CTX-M-64 and CTX-M-14 Provides insights into the structure and catalytic activity of the CTX-M class of enzymes. Antimicrob Agents Chemother 60:6084–6090. https://doi.org/10.1128/AAC.00917-16.
21. He D, Partridge SR, Shen J, Zeng Z, Liu L, Rao L, Lv L, Liu JH. 2013. CTX-M-123, a novel hybrid of the CTX-M-1 and CTX-M-9 group β-lactamases recovered from *Escherichia coli* isolates in China. Antimicrob Agents Chemother 57:4068–4071. https://doi.org/10.1128/AAC.00541-13.
22. Liu L, He D, Lv L, Liu W, Chen X, Zeng Z, Partridge SR, Liu JH. 2015. $bla_{\text{CTX-M-1/9/1}}$ hybrid genes may have been generated from $bla_{\text{CTX-M-15}}$ on an IncI2 plasmid. Antimicrob Agents Chemother 59:4464–4470. https://doi.org/10.1128/AAC.00501-15.
23. Rodriguez MM, Power P, Sader H, Galleni M, Gutkind G. 2010. Novel chromosome-encoded CTX-M-78 β-lactamase from a *Kluyvera georgiana* clinical isolate as a putative origin of CTX-M-25 subgroup. Antimicrob Agents Chemother 54:3070–3071. https://doi.org/10.1128/AAC.01615-09.
24. Dropa M, Ghiglione B, Matte MH, Balsalobre LC, Lincopan N, Matte GR, Gutkind G, Power P. 2015. Molecular and biochemical characterization of CTX-M-131, a natural Asp240Gly variant derived from CTX-M-2, produced by a *Providencia rettgeri* clinical strain in Sao Paulo, Brazil. Antimicrob Agents Chemother 59:1815–1817. https://doi.org/10.1128/AAC.04116-14.
25. Ghiglione B, Rodriguez MM, Herman R, Curto L, Dropa M, Bouillenne F, Kerff F, Galleni M, Charlier P, Gutkind G, Sauvage E, Power P. 2015. Structural and kinetic insights into the "ceftazidimase" behavior of the extended-spectrum β-lactamase CTX-M-96. Biochemistry 54:5072–5082. https://doi.org/10.1021/acs.biochem.5b00313.
26. Ruggiero M, Curto L, Brunetti F, Sauvage E, Galleni M, Power P, Gutkind G. 2017. Impact of mutations at Arg220 and Thr237 in PER-2 β-lactamase on conformation, activity, and susceptibility to inhibitors. Antimicrob Agents Chemother 61:e02193-16. https://doi.org/10.1128/AAC.02193-16.
27. Ruggiero M, Papp-Wallace KM, Taracila MA, Mojica MF, Bethel CR, Rudin

SD, Zeiser ET, Gutkind G, Bonomo RA, Power P. 2017. Exploring the landscape of diazabicyclooctane (DBO) inhibition: avibactam (AVI) inactivation of PER-2 β-lactamase. Antimicrob Agents Chemother 61:e02476-16. https://doi.org/10.1128/AAC.02476-16.
28. Papp-Wallace KM, Winkler ML, Gatta JA, Taracila MA, Chilakala S, Xu Y, Johnson JK, Bonomo RA. 2014. Reclaiming the efficacy of β-lactam-β-lactamase inhibitor combinations: avibactam restores the susceptibility of CMY-2-producing *Escherichia coli* to ceftazidime. Antimicrob Agents Chemother 58:4290–4297. https://doi.org/10.1128/AAC.02625-14.
29. Ibuka AS, Ishii Y, Galleni M, Ishiguro M, Yamaguchi K, Frere JM, Matsuzawa H, Sakai H. 2003. Crystal structure of extended-spectrum β-lactamase Toho-1: insights into the molecular mechanism for catalytic reaction and substrate specificity expansion. Biochemistry 42:10634–10643. https://doi.org/10.1021/bi0342822.
30. Strynadka NC, Adachi H, Jensen SE, Johns K, Sielecki A, Betzel C, Sutoh K, James MN. 1992. Molecular structure of the acyl-enzyme intermediate in β-lactam hydrolysis at 1.7 Å resolution. Nature 359:700–705. https://doi.org/10.1038/359700a0.
31. Fonze E, Vanhove M, Dive G, Sauvage E, Frere JM, Charlier P. 2002. Crystal structures of the *Bacillus licheniformis* BS3 class A β-lactamase and of the acyl-enzyme adduct formed with cefoxitin. Biochemistry 41:1877–1885. https://doi.org/10.1021/bi015789k.
32. Chen Y, Shoichet B, Bonnet R. 2005. Structure, function, and inhibition along the reaction coordinate of CTX-M β-lactamases. J Am Chem Soc 127:5423–5434. https://doi.org/10.1021/ja042850a.
33. Olson AB, Silverman M, Boyd DA, McGeer A, Willey BM, Pong-Porter V, Daneman N, Mulvey MR. 2005. Identification of a progenitor of the CTX-M-9 group of extended-spectrum β-lactamases from *Kluyvera georgiana* isolated in Guyana. Antimicrob Agents Chemother 49:2112–2115. https://doi.org/10.1128/AAC.49.5.2112-2115.2005.
34. Poirel L, Kampfer P, Nordmann P. 2002. Chromosome-encoded Ambler class A β-lactamase of *Kluyvera georgiana*, a probable progenitor of a subgroup of CTX-M extended-spectrum β-lactamases. Antimicrob Agents Chemother 46:4038–4040. https://doi.org/10.1128/aac.46.12.4038-4040.2002.
35. Humeniuk C, Arlet G, Gautier V, Grimont P, Labia R, Philippon A. 2002. β-Lactamases of *Kluyvera ascorbata*, probable progenitors of some plasmid-encoded CTX-M types. Antimicrob Agents Chemother 46:3045–3049. https://doi.org/10.1128/aac.46.9.3045-3049.2002.
36. Peduzzi J, Farzaneh S, Reynaud A, Barthelemy M, Labia R. 1997. Characterization and amino acid sequence analysis of a new oxyimino cephalosporin-hydrolyzing class A β-lactamase from *Serratia fonticola* CUV. Biochim Biophys Acta 1341:58–70. https://doi.org/10.1016/S0167-4838(97)00020-4.
37. Fournier B, Roy PH. 1997. Variability of chromosomally encoded β-lactamases from *Klebsiella oxytoca*. Antimicrob Agents Chemother 41:1641–1648. https://doi.org/10.1128/AAC.41.8.1641.
38. Bellais S, Poirel L, Fortineau N, Decousser JW, Nordmann P. 2001. Biochemical-genetic characterization of the chromosomally encoded extended-spectrum class A β-lactamase from *Rahnella aquatilis*. Antimicrob Agents Chemother 45:2965–2968. https://doi.org/10.1128/AAC.45.10.2965-2968.2001.
39. Matsumoto Y, Inoue M. 1999. Characterization of SFO-1, a plasmid-mediated inducible class A β-lactamase from *Enterobacter cloacae*. Antimicrob Agents Chemother 43:307–313. https://doi.org/10.1128/AAC.43.2.307.
40. Lartigue MF, Nordmann P, Edelstein MV, Cuzon G, Brisse S, Poirel L. 2013. Characterization of an extended-spectrum class A β-lactamase from a novel enterobacterial species taxonomically related to *Rahnella* spp./*Ewingella* spp. J Antimicrob Chemother 68:1733–1736. https://doi.org/10.1093/jac/dkt122.
41. Clinical and Laboratory Standards Institute. 2020. Performance standards for antimicrobial susceptibility testing, 30th ed. Approved standard M100. Clinical and Laboratory Standards Institute, Wayne, PA.
42. Notredame C, Higgins DG, Heringa J. 2000. T-Coffee: a novel method for fast and accurate multiple sequence alignment. J Mol Biol 302:205–217. https://doi.org/10.1006/jmbi.2000.4042.
43. Gouet P, Robert X, Courcelle E. 2003. ESPript/ENDscript: extracting and rendering sequence and 3D information from atomic structures of proteins. Nucleic Acids Res 31:3320–3323. https://doi.org/10.1093/nar/gkg556.
44. Lefort V, Longueville JE, Gascuel O. 2017. SMS: Smart Model Selection in PhyML. Mol Biol Evol 34:2422–2424. https://doi.org/10.1093/molbev/msx149.
45. Guindon S, Dufayard JF, Lefort V, Anisimova M, Hordijk W, Gascuel O. 2010. New algorithms and methods to estimate maximum-likelihood phylogenies: assessing the performance of PhyML 3.0. Syst Biol 59:307–321. https://doi.org/10.1093/sysbio/syq010.
46. Segel IH. 1975. Enzyme kinetics, behavior and analysis of rapid equilibrium and steady-state enzyme systems. John Wiley & Sons, Inc., New York, NY.
47. De Meester F, Joris B, Reckinger G, Bellefroid-Bourguignon C, Frere JM, Waley SG. 1987. Automated analysis of enzyme inactivation phenomena: application to β-lactamases and DD-peptidases. Biochem Pharmacol 36:2393–2403. https://doi.org/10.1016/0006-2952(87)90609-5.
48. Papp-Wallace KM, Bethel CR, Distler AM, Kasuboski C, Taracila M, Bonomo RA. 2010. Inhibitor resistance in the KPC-2 β-lactamase, a preeminent property of this class A β-lactamase. Antimicrob Agents Chemother 54:890–897. https://doi.org/10.1128/AAC.00693-09.
49. Fernea A, Galleni M, Frere JM. 2015. Kinetics of the interaction between avibactam and the CHE-1 class C β-lactamase. J Antimicrob Chemother 70:951–953. https://doi.org/10.1093/jac/dku442.
50. Frere JM, Bogaerts P, Huang TD, Stefanic P, Moray J, Bouillenne F, Brans A. 2020. Interactions between avibactam and ceftazidime-hydrolyzing class D β-lactamases. Biomolecules 10. https://doi.org/10.3390/biom10030483.
51. Power P, Galleni M, Ayala JA, Gutkind G. 2006. Biochemical and molecular characterization of three new variants of AmpC β-lactamases from *Morganella morganii*. Antimicrob Agents Chemother 50:962–967. https://doi.org/10.1128/AAC.50.3.962-967.2006.
52. Kabsch W. 2010. XDS. Acta Crystallogr D Biol Crystallogr 66:125–132. https://doi.org/10.1107/S0907444909047337.
53. McCoy AJ, Grosse-Kunstleve RW, Adams PD, Winn MD, Storoni LC, Read RJ. 2007. Phaser crystallographic software. J Appl Crystallogr 40:658–674. https://doi.org/10.1107/S0021889807021206.
54. Nichols DA, Hargis JC, Sanishvili R, Jaishankar P, Defrees K, Smith EW, Wang KK, Prati F, Renslo AR, Woodcock HL, Chen Y. 2015. Ligand-induced proton transfer and low-barrier hydrogen bond revealed by X-ray crystallography. J Am Chem Soc 137:8086–8095. https://doi.org/10.1021/jacs.5b00749.
55. Adams PD, Afonine PV, Bunkoczi G, Chen VB, Davis IW, Echols N, Headd JJ, Hung LW, Kapral GJ, Grosse-Kunstleve RW, McCoy AJ, Moriarty NW, Oeffner R, Read RJ, Richardson DC, Richardson JS, Terwilliger TC, Zwart PH. 2010. PHENIX: a comprehensive Python-based system for macromolecular structure solution. Acta Crystallogr D Biol Crystallogr 66:213–221. https://doi.org/10.1107/S0907444909052925.
56. Emsley P, Cowtan K. 2004. Coot: model-building tools for molecular graphics. Acta Crystallogr D Biol Crystallogr 60:2126–2132. https://doi.org/10.1107/S0907444904019158.
57. Schrödinger LLC. 2012. The PyMOL molecular graphics system., v1.5.0.4.